

Markov Chain Beam Randomization: a study of the impact of PLANCK beam measurement errors on cosmological parameter estimation

G. Rocha^{1,2}, L. Pagano³, K.M. Górski^{1,2,4}, K.M. Huffenberger⁵, C.R. Lawrence¹, and A.E. Lange²

¹ Jet Propulsion Laboratory, California Institute of Technology, 4800 Oak Grove Drive, Pasadena CA 91109, U.S.A.

² California Institute of Technology, Pasadena CA 91125, U.S.A.

³ Physics Department and sezione INFN, University of Rome “La Sapienza”, Ple Aldo Moro 2, 00185 Rome, Italy.

⁴ Warsaw University Observatory, Aleje Ujazdowskie 4, 00478 Warszawa, Poland.

⁵ Department of Physics, University of Miami, 1320 Campo Sano Avenue, Coral Gables, FL 33124.

Received date / Accepted date

Abstract

We introduce a new method to propagate uncertainties in the beam shapes used to measure the cosmic microwave background to cosmological parameters determined from those measurements. The method, called Markov Chain Beam Randomization (MCBR), randomly samples from a set of templates or functions that describe the beam uncertainties. The method is much faster than direct numerical integration over systematic ‘nuisance’ parameters, and is not restricted to simple, idealized cases as is analytic marginalization. It does not assume the data are normally distributed, and does not require Gaussian priors on the specific systematic uncertainties. We show that MCBR properly accounts for and provides the marginalized errors of the parameters. The method can be generalized and used to propagate any systematic uncertainties for which a set of templates is available. We apply the method to the Planck satellite, and consider future experiments. Beam measurement errors should have a small effect on cosmological parameters as long as the beam fitting is performed after removal of $1/f$ noise.

Key words. Cosmology: cosmic microwave background — Cosmology: observations — Methods: data analysis

1. Introduction

Observations of the cosmic microwave background (CMB) can be interpreted only in light of a detailed knowledge of the angular response of the instrument to radiation, i.e., the shapes of the ‘beams.’ It is almost always the case that the beams from single-aperture telescopes (but not interferometers) can be approximated as two-dimensional Gaussians. It is never the case that a gaussian approximation provides an adequate description of the beams of an experiment that measures the CMB with high signal-to-noise ratio. If the beams were known perfectly, their effects on the data could be calculated perfectly, if painfully. Unfortunately, beams are never known perfectly, and among the outstanding issues for any CMB experiment are how to optimize the beams in the first place, and how to control and account for beam uncertainties in the data analysis.

The effects of beam uncertainties can be analyzed in maps, power spectra, and cosmological parameters determined from the data. Each has benefits. Because cosmological parameters are a key product of any experiment, and because they are sensitive to extremely small effects impossible to detect pixel by pixel, they are particularly valuable. Historically, however, calculation of the effects of beam uncertainties on cosmological parameters has been done either analytically, which requires over-simplified beam shapes, or numerically, at great computational cost.

We introduce in this paper a method for calculating the effects of beam uncertainties on cosmological parameters determined from CMB observations that is both fast and flexible. It requires only that beam uncertainties, or for that matter any other systematic effect, can be represented by a set of functions or templates, which could be obtained from Monte Carlo simulations. It does not assume that the data themselves are Gaussian-distributed, or that the uncertainties have Gaussian priors.

In § II we describe the method, called Markov Chain Beam Randomization or MCBR, and we show that the MCBR technique produces correct marginalized errors. § III summarizes the beam fitting procedure developed in a previous paper (Huffenberger et al. 2009). § IV describes the implementation of MCBR. In § VI we apply the method to the Planck experiment, and consider future experiments.

2. MCBR: Markov Chain Beam Randomization

In the past, marginalization over systematic parameters has been carried out either numerically or analytically (Bridle et al. 2002); both methods are currently implemented in *cosmomc* (Lewis and Bridle 2002). Assuming likelihoods are Gaussian one typically has a marginalization of the form:

$$L \propto \int d\alpha P(\alpha) \exp[-(\alpha\mathbf{v} - \mathbf{d})^T \mathbf{N}^{-1}(\alpha\mathbf{v} - \mathbf{d})/2] \quad (1)$$

where \mathbf{d} is the theoretical (predicted) data minus the observed data and $\alpha\mathbf{v}$ is an approximate template describing the correction applied to the predicted data due to systematics, \mathbf{N} is the noise covariance matrix, and $P(\alpha)$ is the prior. The marginalization is given by:

$$-2 \ln L = \mathbf{d}^T \left(\mathbf{N}^{-1} - \frac{\mathbf{N}^{-1} \mathbf{v} \mathbf{v}^T \mathbf{N}^{-1}}{\mathbf{v}^T \mathbf{N}^{-1} \mathbf{v}} \right) \mathbf{d} + \ln(\mathbf{v}^T \mathbf{N}^{-1} \mathbf{v}) + c \quad (2)$$

where c is a constant. If \mathbf{v} is independent of the data and parameters then $L \propto e^{-\chi_{eff}^2/2}$, with:

$$\chi_{eff}^2 = \mathbf{d}^T \left(\mathbf{N}^{-1} - \frac{\mathbf{N}^{-1} \mathbf{v} \mathbf{v}^T \mathbf{N}^{-1}}{\mathbf{v}^T \mathbf{N}^{-1} \mathbf{v}} \right) \mathbf{d} = \chi_{best-fit}^2 \quad (3)$$

In the case of beam uncertainties, the analytic approach is feasible only if the beams are assumed to be Gaussian. This is not realistic.

It is customary to characterize anisotropies in the Cosmic Microwave Background by their angular power spectrum, \mathbf{C}_ℓ for both temperature and polarization. \mathbf{C}_ℓ is a 3×3 matrix for T (temperature) and E or B (grad-type or curl-type polarization):

$$\mathbf{C}_\ell = \begin{pmatrix} C_\ell^{TT} & C_\ell^{TE} & C_\ell^{TB} \\ C_\ell^{TE} & C_\ell^{EE} & C_\ell^{EB} \\ C_\ell^{TB} & C_\ell^{EB} & C_\ell^{BB} \end{pmatrix}, \quad (4)$$

Hereafter, for the sake of simplicity, most equations will refer to the angular power spectrum, C_ℓ , for a single component, say temperature. The telescope beam smooths the anisotropies, suppressing power at higher multipoles. We refer to the ratio of the measured power spectrum of the sky and our true power spectrum as the transfer function, $\mathcal{B}_\ell = B_\ell^2$. Here we assume the beam transfer functions are the same for temperature and polarization.

To obtain unbiased estimates of the parameters that characterize the cosmology, we must repair this suppression based on knowledge of the beam. Uncertainties in the beam propagate into uncertainties in the cosmological parameters.

We assume that the beam uncertainties can be described by a set of functions or templates, taken here to be the set of transfer functions obtained by the beam fitting procedure described in § 3. These templates are given in multipole space by:

$$\mathcal{B}_\ell^r = (B_\ell^r)^2 = (B_\ell \times r_\ell)^2 \quad (5)$$

where the ratios r_ℓ represent the possible deviations from the true fiducial beam. We choose the beam transfer function randomly from the set of N simulations (here $N = 1280$) for each step of the Markov Chain Monte Carlo when probing the cosmological parameters space. This means that at each step of the chain the theoretical power spectrum, \mathbf{C}_ℓ , is multiplied by the randomly chosen beam, \mathcal{B}_ℓ^r . We assume all transfer functions in the set are equally probable.

To estimate constraints on cosmological parameters, we need to compare the model with the data via a chosen Likelihood and an algorithm to sample cosmological parameters. Here we make use of the package `cosmomc`. To incorporate MCBR we modify `cosmomc` to enable the usage of a random \mathcal{B}_ℓ^r for each theoretical model generated with CAMB (Lewis et al. 2000) or PICO (Fendt and Wandelt 2006). This is done by modifying the `cmbdata` module of the `cosmomc` code.

We start by creating simulated datasets with noise properties specific to the instrument under consideration, in our case Planck and an example of a future experiment (see § 4). These simulated datasets are given in terms of the angular Power Spectrum C_ℓ^{obs} :

$$C_\ell^{obs} = C_\ell^{wmap} \mathcal{B}_\ell + \mathcal{N}_\ell \quad (6)$$

where \mathcal{N}_ℓ is the noise power spectrum and $\mathcal{B}_\ell = B_\ell^2$ is the beam transfer function and C_ℓ^{wmap} is the Λ CDM spectrum best-fitting current WMAP data. In the case of a symmetric Gaussian beam, $B(\mathbf{x}) = \frac{1}{2\pi\sigma^2} \exp\left\{-\frac{|\mathbf{x}|^2}{2\sigma^2}\right\}$, so that $B_\ell = e^{-\frac{1}{2}\sigma^2\ell^2}$. However, the Planck beams are not adequately represented by Gaussians. Instead, we use realistic beams calculated from a full diffraction analysis of the telescope using GRASP9 (Sandri et al. 2002, Sandri et al 2009, Maffei et al. 2009, Yurchenko et al. 2004).

As our purpose here is to introduce and validate the MCBR method it suffices to assume full-sky coverage. Considerations of realistic complications (such as cut-sky, foregrounds, etc.) is deferred to a future publication. Our purpose here is to establish the relative importance of propagating beam errors to cosmological parameters rather than to make comprehensive predictions for Planck. Hereafter to compare the observed dataset, \mathbf{C}_ℓ^{obs} , with theoretical models we use the exact full-sky likelihood (with $\hat{\mathbf{C}}_\ell = \mathbf{C}_\ell^{obs}$) (Bond, Jaffe and Knox 2000):

$$-2 \ln L(\hat{\mathbf{C}}_\ell | \mathbf{C}_\ell) = (2\ell + 1) \left(\ln |\mathbf{C}_\ell| + \text{Tr} \left(\hat{\mathbf{C}}_\ell \mathbf{C}_\ell^{-1} \right) \right), \quad (7)$$

i.e., the Inverse Wishart distribution for Temperature and Polarization. In `cosmomc` this distribution is coded in function `ChiSqExact` (Lewis 2005). We analyse these datasets with a modified version of this function, built to include the MCBR procedure in the code.

The C_ℓ of the theoretical model is given by:

$$\tilde{C}_\ell = C_\ell \times \mathcal{B}_\ell^r \quad (8)$$

where \mathcal{B}_ℓ^r is the randomly chosen transfer function. To incorporate both the beam and the uniform white noise in the likelihood expression one should replace:

$$\hat{C}_\ell \rightarrow C_\ell^{obs} \quad (9)$$

$$C_\ell \rightarrow C_\ell^{th} \times \mathcal{B}_\ell^r + \mathcal{N}_\ell \quad (10)$$

where C_ℓ^{obs} is given by Equation 6, C_ℓ^{th} is the theoretical power spectrum computed e.g. by CAMB, and \mathcal{B}_ℓ^r is the randomly chosen beam transfer function.

In the MCBR scheme, sampling of the beam templates is equivalent to sampling from the proposal distribution. The Metropolis-Hastings algorithm accepts the move from θ_n to θ_{n+1} in the Markov chain by evaluating the ratio:

$$\frac{P(\theta_{n+1})q(\theta_{n+1}, \theta_n)}{P(\theta_n)q(\theta_n, \theta_{n+1})} \quad (11)$$

where P is the posterior distribution we wish to sample from and q is the proposal distribution. We draw the proposal at position θ_n of the parameter space from $q(\theta_{n+1}, \theta_n)$. Here $\theta = (\theta_{cp}, \theta_b)$, with θ_{cp} the subset of cosmological parameters and θ_b the beam parameter. The joint proposal density for θ factors into

$$q(\theta_{n+1}, \theta_n) = q_{cp}(\theta_{cp,n+1}, \theta_{cp,n})q_b(\theta_{b,n+1}, \theta_{b,n}), \quad (12)$$

where $\theta_{cp,n+1}$ refers to $(\theta_{cp})_{n+1}$ and $\theta_{b,n+1}$ to $(\theta_b)_{n+1}$. Now, we take the $q_b(\theta_{b,n+1}, \theta_{b,n})$ to be the posterior distribution of the beam parameters given the beam fitting data (in our case the Jupiter beam fitting data (see § 3)), i.e.,

$$q_b(\theta_{b,n+1}, \theta_{b,n}) = P_b(\theta_{b,n}|\text{beamdata}) \quad (13)$$

Furthermore

$$P(\theta_{n+1}) = P_{cp}(\theta_{n+1}|\text{mapdata})P_b(\theta_{b,n+1}|\text{beamdata}) \quad (14)$$

(for instance in our study here $P_{cp}(\theta|\text{mapdata}) = L(\text{mapdata}|\theta_{cp}, \theta_b)p_{cp}(\theta_{cp})$ where L is the Likelihood given in Equation 7 and p_{cp} the prior on cosmological parameters.) Hence the ratio in Equation 11 becomes:

$$\frac{P_{cp}(\theta_{n+1})q_{cp}(\theta_{cp,n+1}, \theta_{cp,n})}{P_{cp}(\theta_n)q_{cp}(\theta_{cp,n}, \theta_{cp,n+1})} \quad (15)$$

as P_b and q_b cancel out.

Hence random sampling from the set of beam templates at each step of the Markov chain is equivalent to sampling from a proposal density that, by construction, is identical to the posterior distribution of the beam parameters given the beam fitting data.

To illustrate how the MCBR procedure works, we give here the steps followed in our analysis (see section 5). We start by comparing two cases:

1. cosmomc run with the ‘true’ fiducial beam transfer alone, \mathcal{B}_ℓ .
2. cosmomc run with the MCBR procedure for the set of beam transfer functions, \mathcal{B}_ℓ^r , obtained from the beam fitting step.

To this end:

- We generate a simulated data set using as fiducial the ‘true’ beam transfer \mathcal{B}_ℓ
- We analyse this simulated data set with cosmomc, including in the code just the effect of the \mathcal{B}_ℓ (ie the theoretical C_ℓ is multiplied by the true beam transfer, \mathcal{B}_ℓ)
- We analyse this simulated data set with a modified version of cosmomc in which the theoretical C_ℓ is multiplied by the randomly chosen beam, \mathcal{B}_ℓ^r at each step of the chain—i.e., with in-built MCBR

The MCBR method can be used to propagate any systematic uncertainties that can be characterized by a set of templates. We turn these into multiplicative and additive corrections to the C_ℓ , encode the corrected C_ℓ into the likelihood, and randomly sample from the set of templates at the Markov Chain Monte Carlo step of parameter estimation. The data do not have to be normally distributed. Furthermore, unlike analytic marginalization, the method does not require Gaussian priors on the uncertainties.

2.1. Validation

To demonstrate that the MCBR technique gives correct marginalized errors, we compared the results given by MCBR to those from a ‘brute force’ cosmomc calculation in which the beam was taken as another parameter. We did this for three simulated datasets, the first generated using the ‘true’ beam transfer function \mathcal{B}_ℓ , the second and third using beam transfer functions that were chosen to be mildly and extremely far from the true one, respectively. We simplified the test cases by assuming that the beam was a symmetric 7' (FWHM) Gaussian, with 4% variations of the fwhm of the beam.

The brute force calculation was done by probing the beam parameter space in cosmomc in the same way as for any of the other parameters, and considering the default proposal density already implemented in cosmomc. The beam parameter is included by transforming the theoretical $C_\ell(\theta_{cp})$ output by CAMB at each Markov chain step into

$$C_\ell(\theta_{cp}, \theta_b) = C_\ell(\theta_{cp}) \times \mathcal{B}_\ell^r + \mathcal{N}_\ell, \quad (16)$$

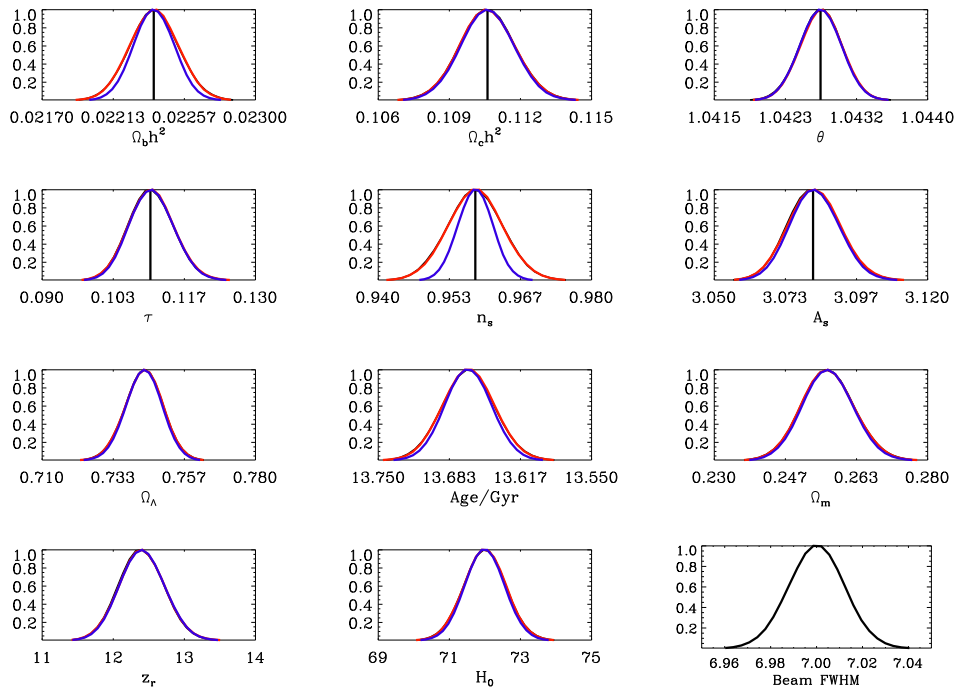


Figure 1. Marginalized parameter constraints for Planck 143 GHz with 7' beam with 4% variations, for the analysis with the ‘true’ reference fiducial beam using beamparameter approach (black) and MCBR (red), the blue line is the analysis of the same dataset without including the beam uncertainty.

where fwhm_n is the width of B_ℓ^n , the Gaussian beam currently sampled. This theoretical $C_\ell(\theta_{cp}, \theta_b)$ is used in the Likelihood expression. To move the Markov chain to the next position in parameter space we use the default proposal density in `cosmomc`, usually an N -d Gaussian. The proposed new point is accepted/rejected following the same prescription used for the other cosmological parameters. A final marginalized distribution of the beam is output along with the other cosmological parameter constraints.

For the MCBR calculation we analysed the simulated data with a modified version of `cosmomc` in which the theoretical C_ℓ is multiplied by the randomly chosen beam transfer, B_ℓ^r at each step of the chain.

The results are plotted in Figures 1, 2, and 3. In all cases, we find same parameter distributions for both methods. As expected, the extreme deviated beam results in a biased estimation of parameters, especially n_s , but equally for both the ‘beamparameter’ and the MCBR procedures.

3. Beam fits and transfer function ensembles

We characterize the beam uncertainty for Planck with a Monte Carlo ensemble of transfer functions (Huffenberger et al. 2009) generated by repeated simulation of Jupiter observations using the detector noise and pointing errors expected before flight. Each realization yields a representative transfer function. The beams are calculated with GRASP9 (Sandri et al. 2002, Sandri et al. 2009, Maffei et al. 2009, Yurchenko et al. 2004), and we employ two methods of beam reconstruction to reproduce them from the planet scans. The first uses a rigid linearized parametric model; the second expands the beam in orthogonal functions (see Rocha et al. 2001 for a previous application of such functions in CMB analysis). Figure 5 shows the nominal Gaussian beams with blue-book fwhm values to that of the fiducial realistic Grasp beams based on a Gaussian fit (see table 1). From the beam reconstruction procedure presented in Huffenberger et al. 2009 we obtain the ratio of the power spectrum as corrected with the fitted beam to the power spectrum as it should have been corrected by the true beam. In Figure 4 we display lines which bound 68% of the ensemble transfer functions for Planck channels.

The simulation of repeated Jupiter calibrations is done in such way that each template is an unbiased estimator of the true template. But in real life, they could be a biased estimator (for instance the Planck pointing error could bias the beam function always in the same direction). This prompted us to consider the runs presented in Section 5.2.

The Beam fitting is applied to data with white + $1/f$ noise, and to destriped data, i.e., after application e.g of a “de-striping” mapmaking code which removes almost all of the effects of $1/f$ noise [Poutanen et al. 2006, Ashdown et al. 2007a, Ashdown et al. 2007b, Ashdown et al. 2009]. We use realistic Grasp beams and the parametric model of the reconstructed beams (the results with non-parametric model will be presented in a future paper). Figure 6 shows extreme and mild beam transfer functions for the Planck 70 GHz, 100 GHz, 143 GHz and 217 GHz channels obtained from the beam fitting procedure applied to destriped data (hence containing a very low level of $1/f$ residuals). For comparison purposes we plot in Figure 7 these functions obtained from data with a white and $1/f$ noise background. We also plot in Figures 8 the normalized histograms of the ratios, r_ℓ^2 , for single multipoles $\ell = 500, 1000, 1500, 2000$. For all channels the distributions are slightly skewed and get broader with increasing multipole ℓ

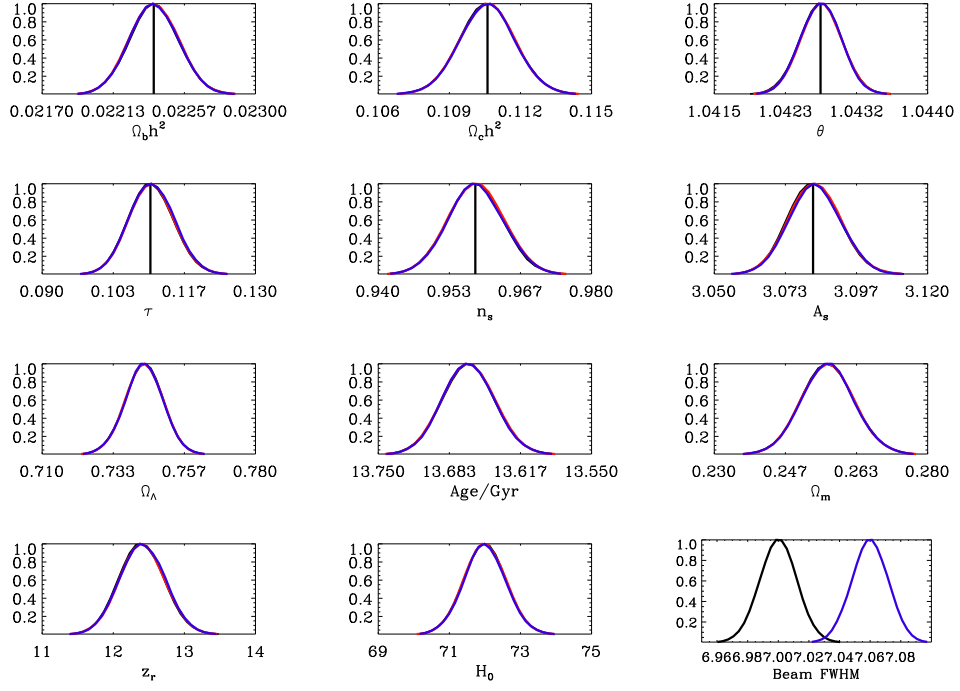


Figure 2. Marginalized parameter constraints for Planck 143 GHz with 7' beam with 4% variations, for the analysis with the ‘true’ reference fiducial beam (black) and for the mildly deviated beam transfer, $\mathcal{B}_\ell^{mild} = (B_\ell \times r_\ell^{mild})^2$, using beamparameter approach (blue) and MCBR (red), both beamparameter and MCBR give same distributions

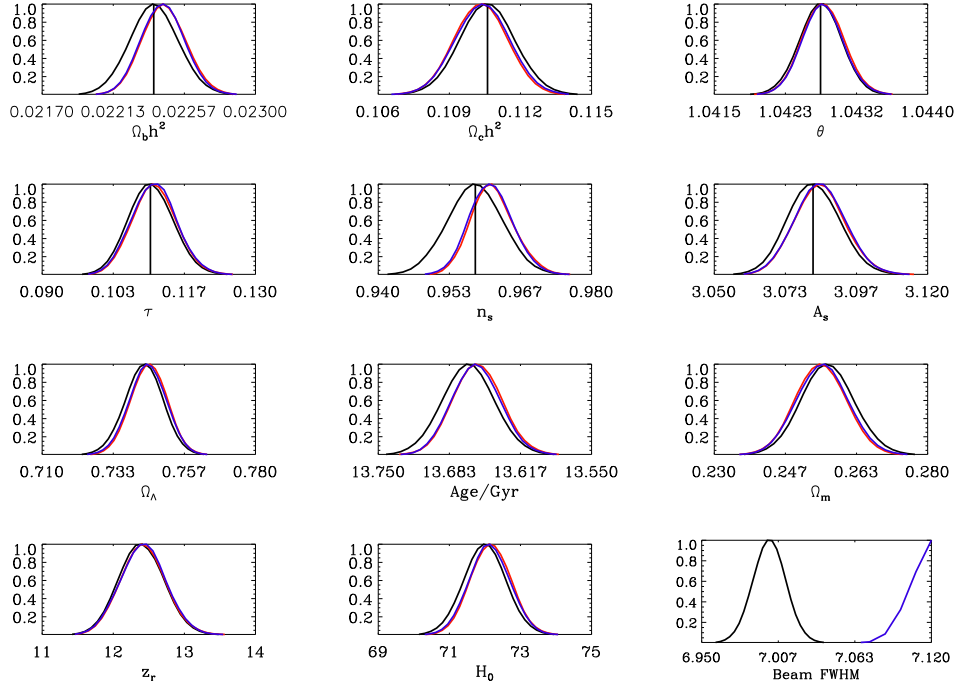


Figure 3. Marginalized parameter constraints for Planck 143 GHz with 7' beam with 4% variations, for the analysis with the ‘true’ reference fiducial beam (black) and for the extremely deviated fiducial beam, $\mathcal{B}_\ell^{ext} = (B_\ell \times r_\ell^{ext})^2$, using beamparameter approach (blue) and MCBR (red), both beamparameter and MCBR give same distributions.

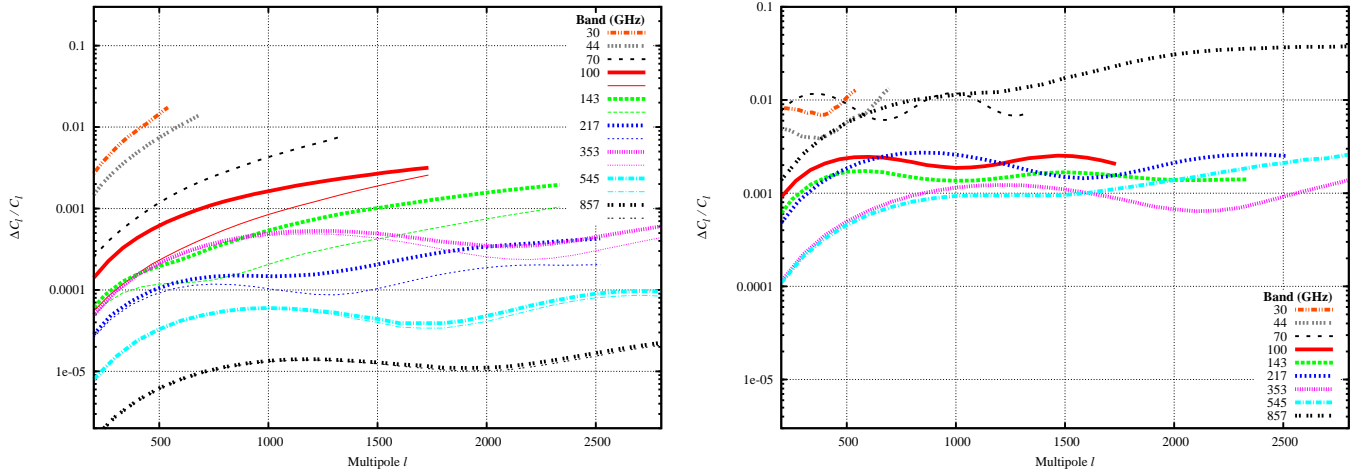


Figure 4. At each multipole, 68% of the fitted Monte Carlo transfer functions recover spectra closer to the true power spectrum than the indicated line. Left: parametric model. Right: non-parametric model based on orthogonal functions, where the flexibility requires less knowledge of the beam, but yields larger errors.

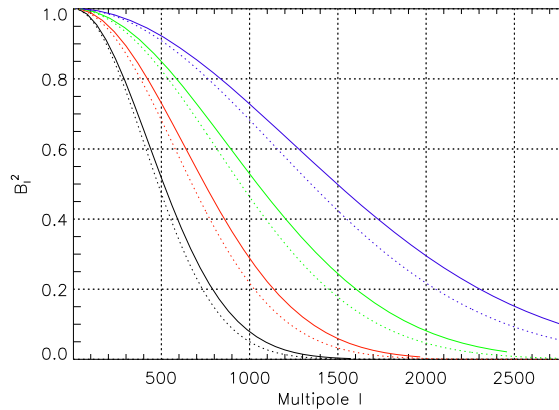


Figure 5. Nominal Gaussian blue-book beams (dotted line) vs Fiducial realistic Grasp9 beams based on a Gaussian fit (solid line) for 70GHz (black), 100GHz (red), 143GHz (green) and 217GHz(blue).

for each channel. We can also compare the probability of the mildly deviated and extremely deviated transfer functions used in § 5. For instance for 70 GHz for $\ell = 1000$ the mild function is $\approx 10\%$ probable while the extreme function is approximately 100 times less likely. The maximum variation for transfer function ratios, r_l^2 , is of the order 2% for 70 GHz (0.5% for 100GHz) for destriped data, while for white and $1/f$ noise data with no attempt at destriping it increases to $\sim 30\%$ for the 70 GHz channel ($\sim 2.5\%$ for 100 GHz).

In § 5 we infer that the parameter constraints from beams obtained with destriped data are slightly worse but very close to those obtained with a white noise background as expected.

4. Analysis: from Beam transfer function uncertainties to parameter estimation

To propagate the beam measurement errors to parameters we apply the MCBR method following the procedure described in § 2. We make use of the beam transfer functions obtained with the beam fitting described in § 3. For this purpose we use a modified version of `cosmomc` with built-in MCBR step as described in § 2. We consider a set of five chains. The convergence diagnostic is based on the Gelman and Rubin statistic, as usual in the field. Following MCBR, we choose randomly the beam transfer function (from the set of 1280 simulations) for each step of the Markov Chain. We sample a six-dimensional set of cosmological parameters, with flat priors: the physical baryon and Cold Dark Matter densities, $\omega_b = \Omega_b h^2$ and $\omega_c = \Omega_c h^2$; the ratio of the sound horizon to the angular diameter distance at decoupling, θ_s ; the scalar spectral index n_s ; the overall normalization of the spectrum $\log[10^{10}A]$ at $k = 0.05 \text{ Mpc}^{-1}$ (hereafter A_S), and the optical depth to reionization τ . We use a cosmic age top-hat prior $10 \text{ Gyr} \leq t_0 \leq 20 \text{ Gyr}$, consider purely adiabatic initial conditions only, we impose flatness, and we treat the dark energy component as a cosmological constant.

We create simulated datasets with the noise properties of the Planck 70, 100, 143 and 217 GHz (Planck Blue Book 2005) channels, as well as one example of a future experiment. For the latter we considered the noise levels of Epic 150 GHz (Bock et al. 2008). We take as our cosmological model the best fit of WMAP 1yr: $\Omega_b h^2 = 0.02238$; $\Omega_c h^2 = 0.11061$; $H_0 = 71.992$; $\tau = 0.110267$;

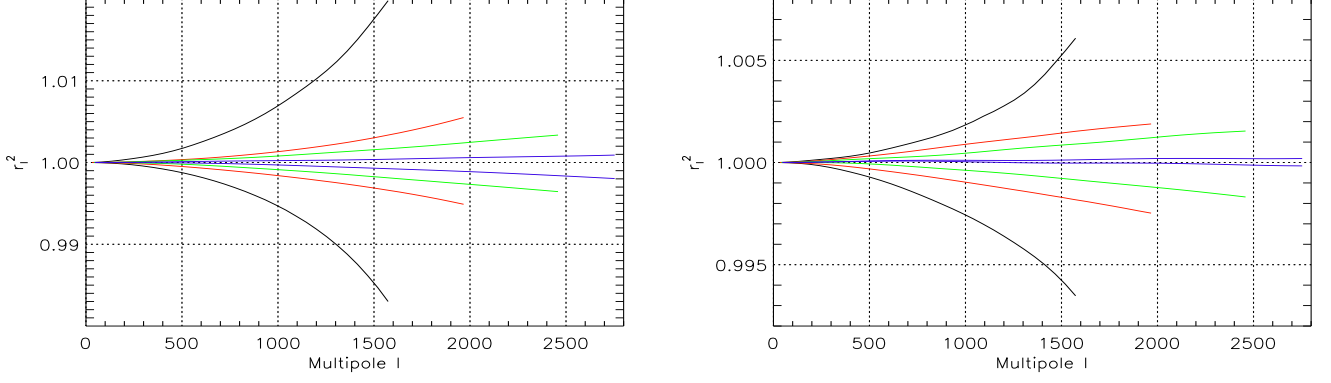


Figure 6. Extreme (left) and Mild (right) beam transfer functions for the Planck 70 GHz (black), 100 GHz (red), 143 GHz (green) and 217 GHz (blue) channels obtained from beam fitting applied to destriped data.

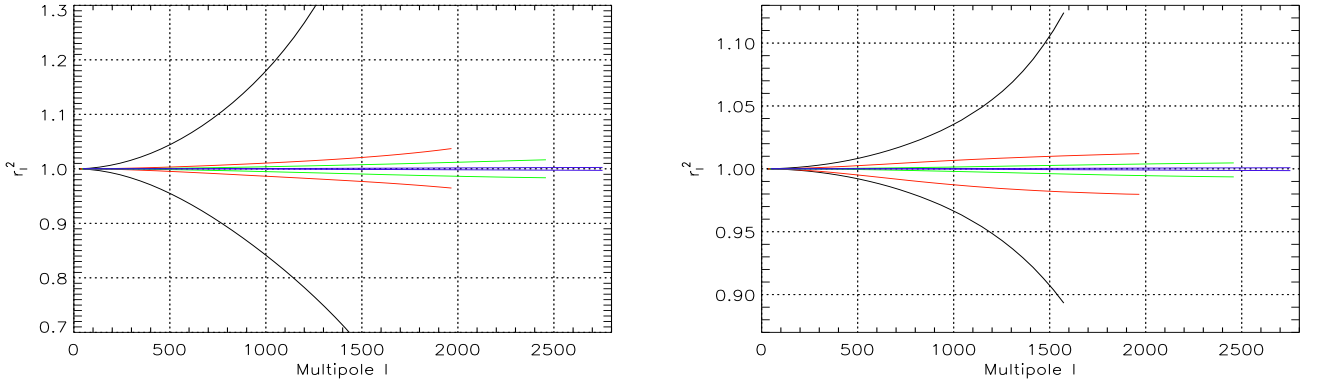


Figure 7. Extreme (left) and Mild (right) beam transfer functions for the Planck 70 GHz (black), 100 GHz (red), 143 GHz (green) and 217 GHz (blue) channels obtained from beam fitting applied to data with white + $1/f$ noise.

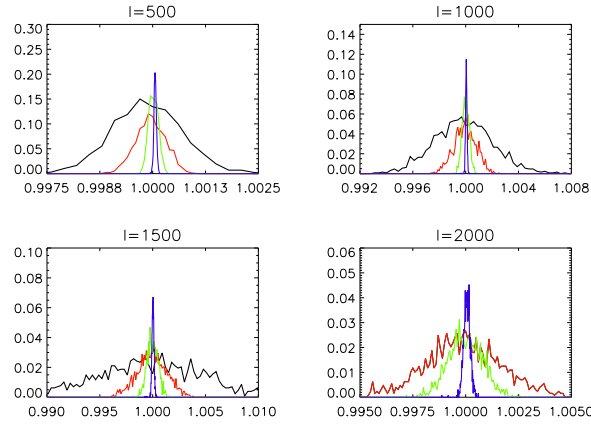


Figure 8. Normalized distributions of the beam transfer functions, $\mathcal{B}_\ell = (B_\ell^r)^2$ for multipoles $\ell = 500, 1000, 1500, 2000$ for 70 GHz (black), 100 GHz (red), 143 GHz (green), and 217 GHz (blue) obtained from the beam fitting on destriped data.

$n_S = 0.95820$; and $A_S = 3.0824$ (Spergel et al. 2003). These simulated datasets are given in terms of the angular Power Spectrum C_ℓ^{obs} as described in § 2. We compute the noise $\mathcal{N}_\ell = (\Delta T \times fwhm)^2$ for Planck and Epic from the sensitivity $\Delta T/T$ and the nominal $fwhm$ of the beam assuming a Gaussian profile (tabulated in Table 1). In Figure 9 we plot the theoretical model vs. the noise levels for each channel considered. Results from this analysis are given in § 5.

| Experiment | Channel | FWHM | $\Delta T/T$ | FWHM (grasp) |
|------------|---------|------|--------------|--------------|
| Planck | 70 | 14' | 4.7 | 13' |
| | 100 | 10' | 2.5 | 9.22' |
| | 143 | 7.1' | 2.2 | 6.49' |
| | 217 | 5.0' | 4.8 | 4.48' |
| Epic-CS | 150 | 5.0' | 0.81 | |

Table 1. Planck (Planck Blue Book 2005) and Epic (Bock et al. 2008) experimental specifications. Channel frequency is given in GHz, FWHM in arcminutes and noise in 10^{-6} . The last column gives the fwhm of our fiducial beams based on a Gaussian fit to the realistic GRASP beams.

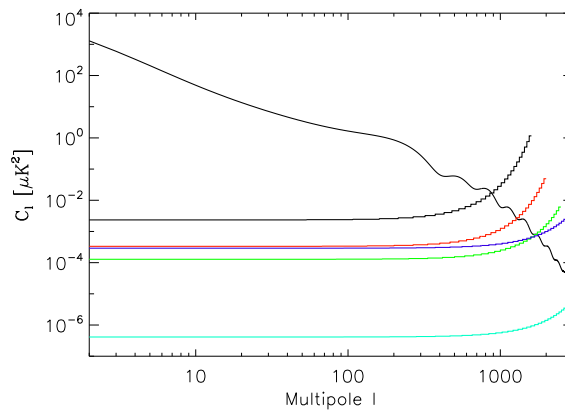


Figure 9. CMB angular power spectrum (best fit of WMAP 1yr, black line) and noise levels for Planck: 70 GHz (black), 100 GHz (red), 143 GHz (green), 217 GHz (blue) and for Epic 150 GHz (cyan).

5. Results

5.1. Results: effect of beam uncertainties

Figures 10, 11, 12, 13 show the marginalized parameter constraints for Planck in three cases: without beam uncertainty (i.e., considering the true fiducial beam) (black); with beam uncertainty using the beam transfer functions obtained using the destriped data (red); and in the presence of $1/f$ noise (blue). Table 2 gives the input cosmological parameters and the mean values and marginalized 68% confidence limits obtained after accounting for the beam errors. To facilitate comparisons, Figure 14 shows these same marginalized constraints for n_s and A_s , the parameters where the largest differences are seen between the three cases.

Equivalent results for a more sensitive polarization experiment—Epic 150 GHz—are plotted in Figure 15; corresponding parameter values are given in table 2.

The most noticeable effect of beam uncertainties is to widen the marginal distributions of some parameters, especially n_s , for uncertainties obtained in the presence of $1/f$ noise but without destriping. A_s , and $\Omega_b h^2$ are also affected. In this case the distribution of the fitted beam transfer functions is wider than that obtained from white noise or destriped data as shown in Figures 6 and 7.

Define σ_{ch} , the width of the distribution when beam errors are marginalised by applying MCBR, and σ_{ref} , the width of the distribution for the simulated data convolved with the fiducial beam (with no beam errors included). Figure 16 shows the enhancement factor, σ_{ch}/σ_{ref} , for parameters n_s and A_s for beams fitted on data with white + $1/f$ noise. For example, at 100 GHz the distributions of n_s and A_s widen by 25% and 11%, respectively.

This widening is much reduced by the use of destriping techniques. For example, with destriping the uncertainties in the beams are 0.5% for 100 GHz at $\ell = 1500$, which translates into an increase of parameter uncertainties of 0.1%. Without destriping, the uncertainties on A_s at 70 GHz and on n_s at 100 GHz increase by 21% and 25%, respectively, for beams fitted on white + $1/f$ noise data. This is a convincing demonstration of the relevance and power of destriping techniques in reducing the effect of $1/f$ noise for Planck.

5.2. Results: effect of assuming a wrong fiducial beam

To illustrate the effect of incorrect beam assumptions we calculated parameters assuming a mildly and then an extremely ‘wrong’ beam. Specifically, we generated three simulated datasets, using: \mathcal{B}_ℓ ; a mildly wrong beam \mathcal{B}_ℓ^{mild} ; and an extremely wrong beam \mathcal{B}_ℓ^{ext} . We analyzed these datasets with the modified version of cosmomc with MCBR built in, and compared the cosmological parameters from the run with for the ‘true’ fiducial beam \mathcal{B}_ℓ to those of both the mild and extreme deviated beams

Figures 17,18,19,20 show marginalized parameter constraints from 70 GHz, 100 GHz, 143 GHz, and 217 GHz, respectively, on destriped data. We see that assuming an extreme beam deviation in the simulated data results in a biased estimation of some

| Channel | Parameter | no beam uncertainty | destriped | white noise+1/f |
|----------------|----------------|-------------------------|-------------------------|-------------------------|
| Planck 70 GHz | $\Omega_b h^2$ | 0.22393 ± 0.00035 | 0.22401 ± 0.00035 | 0.22394 ± 0.00036 |
| | $\Omega_c h^2$ | 0.1106 ± 0.0027 | 0.1105 ± 0.0027 | 0.1106 ± 0.0029 |
| | θ | 1.0428 ± 0.0010 | 1.0428 ± 0.0010 | 1.0428 ± 0.0010 |
| | τ | 0.1112 ± 0.0091 | 0.1111 ± 0.0091 | 0.1112 ± 0.0091 |
| | n_s | 0.959 ± 0.010 | 0.959 ± 0.010 | 0.959 ± 0.011 |
| | A_s | 3.084 ± 0.017 | 3.084 ± 0.017 | 3.084 ± 0.021 |
| Planck 100 GHz | $\Omega_b h^2$ | 0.22383 ± 0.00018 | 0.22383 ± 0.00018 | 0.22383 ± 0.00018 |
| | $\Omega_c h^2$ | 0.1106 ± 0.0015 | 0.1106 ± 0.0015 | 0.1106 ± 0.0015 |
| | θ | 1.04275 ± 0.00038 | 1.04275 ± 0.00038 | 1.04275 ± 0.00038 |
| | τ | 0.1107 ± 0.0049 | 0.1106 ± 0.0049 | 0.1106 ± 0.0049 |
| | n_s | 0.9583 ± 0.0046 | 0.9583 ± 0.0046 | 0.9583 ± 0.0058 |
| | A_s | 3.0832 ± 0.0094 | 3.0831 ± 0.0094 | 3.083 ± 0.011 |
| Planck 143 GHz | $\Omega_b h^2$ | 0.22381 ± 0.00011 | 0.22381 ± 0.00011 | 0.22381 ± 0.00011 |
| | $\Omega_c h^2$ | 0.1106 ± 0.0010 | 0.1106 ± 0.0010 | 0.1106 ± 0.0010 |
| | θ | 1.04275 ± 0.00021 | 1.04275 ± 0.00021 | 1.04274 ± 0.00021 |
| | τ | 0.1105 ± 0.0038 | 0.1105 ± 0.0038 | 0.1105 ± 0.0039 |
| | n_s | 0.9582 ± 0.0029 | 0.9582 ± 0.0029 | 0.9582 ± 0.0035 |
| | A_s | 3.0829 ± 0.0074 | 3.0828 ± 0.0075 | 3.0829 ± 0.0077 |
| Planck 217 GHz | $\Omega_b h^2$ | 0.22380 ± 0.00012 | 0.22382 ± 0.00012 | 0.22383 ± 0.00012 |
| | $\Omega_c h^2$ | 0.1106 ± 0.0012 | 0.1106 ± 0.0012 | 0.1106 ± 0.0012 |
| | θ | 1.04275 ± 0.00023 | 1.04275 ± 0.00023 | 1.04275 ± 0.00024 |
| | τ | 0.1106 ± 0.0046 | 0.1106 ± 0.0046 | 0.1107 ± 0.0047 |
| | n_s | 0.9582 ± 0.0032 | 0.9583 ± 0.0032 | 0.9583 ± 0.0032 |
| | A_s | 3.0831 ± 0.0090 | 3.0830 ± 0.0090 | 3.0831 ± 0.0090 |
| Epic 150 GHz | $\Omega_b h^2$ | 0.223802 ± 0.000029 | 0.223798 ± 0.000029 | 0.223802 ± 0.000029 |
| | $\Omega_c h^2$ | 0.11061 ± 0.00051 | 0.11061 ± 0.00051 | 0.11061 ± 0.00052 |
| | θ | 1.042750 ± 0.000054 | 1.042750 ± 0.000054 | 1.042750 ± 0.000054 |
| | τ | 0.1104 ± 0.0023 | 0.1103 ± 0.0023 | 0.1103 ± 0.0024 |
| | n_s | 0.9582 ± 0.0016 | 0.9582 ± 0.0016 | 0.9583 ± 0.0016 |
| | A_s | 3.0827 ± 0.0047 | 3.0825 ± 0.0047 | 3.083 ± 0.0047 |

Table 2. Mean values and marginalized 68% c.l. limits using the fiducial beam: analysis without beam uncertainty (column 3), accounting the beam uncertainty from destriped data (column 4) and from the data with white and 1/f noise (column 5).

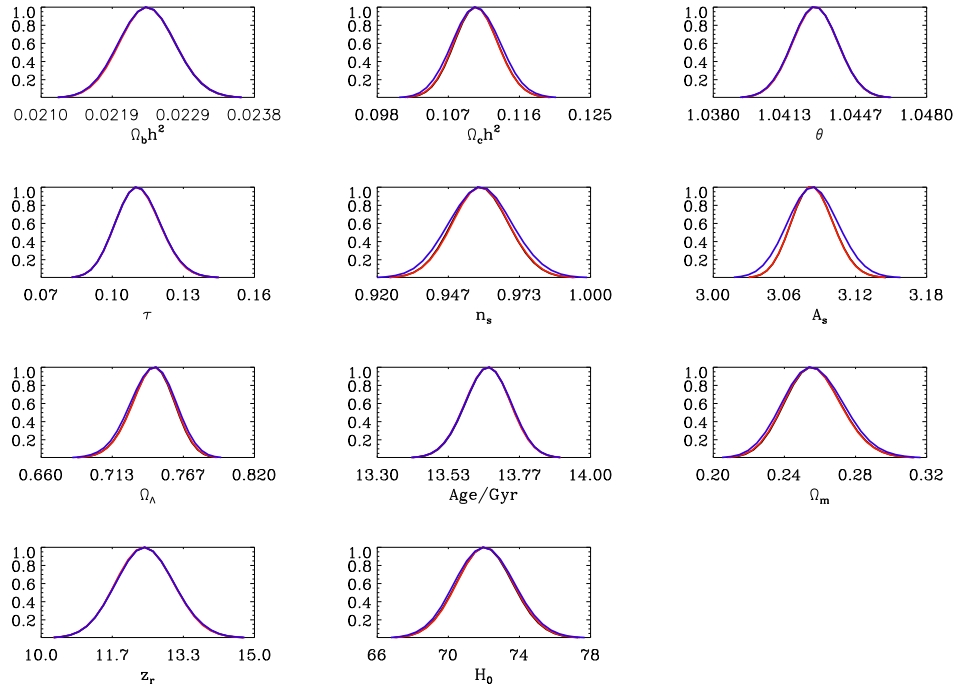


Figure 10. Marginalized parameter constraints for Planck 70 GHz without beam uncertainty (black), marginalized over the beam uncertainty via MCBR considering the destriped data (red), and in the presence of white noise +1/f noise (blue).

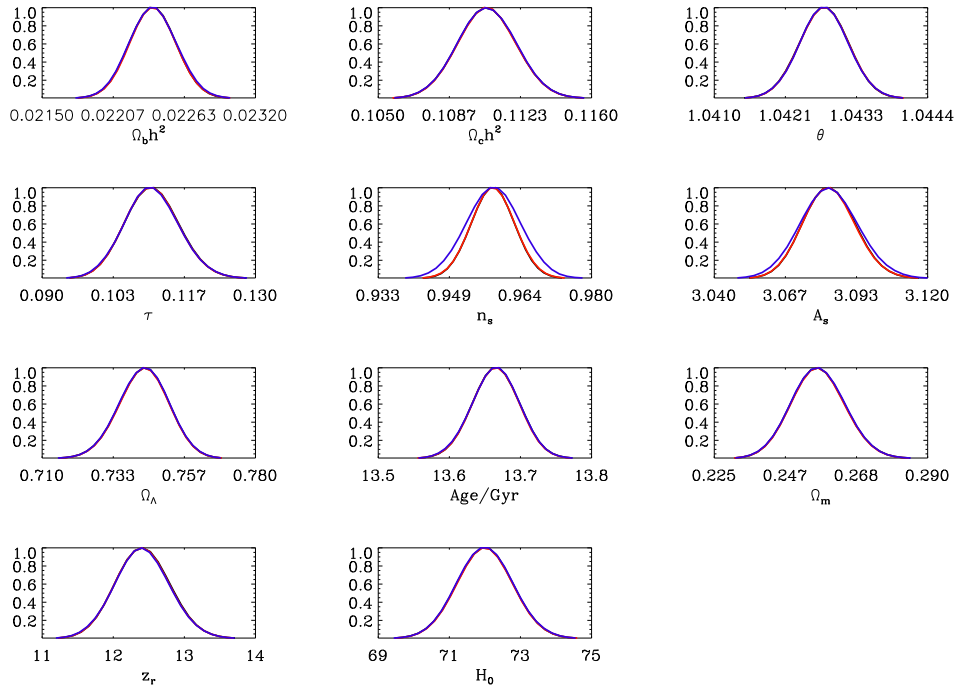


Figure 11. Marginalized parameter constraints for Planck 100 GHz without beam uncertainty (black), marginalized over the beam uncertainty via MCBR considering the destriped data (red) and in the presence of white noise + $1/f$ noise (blue).

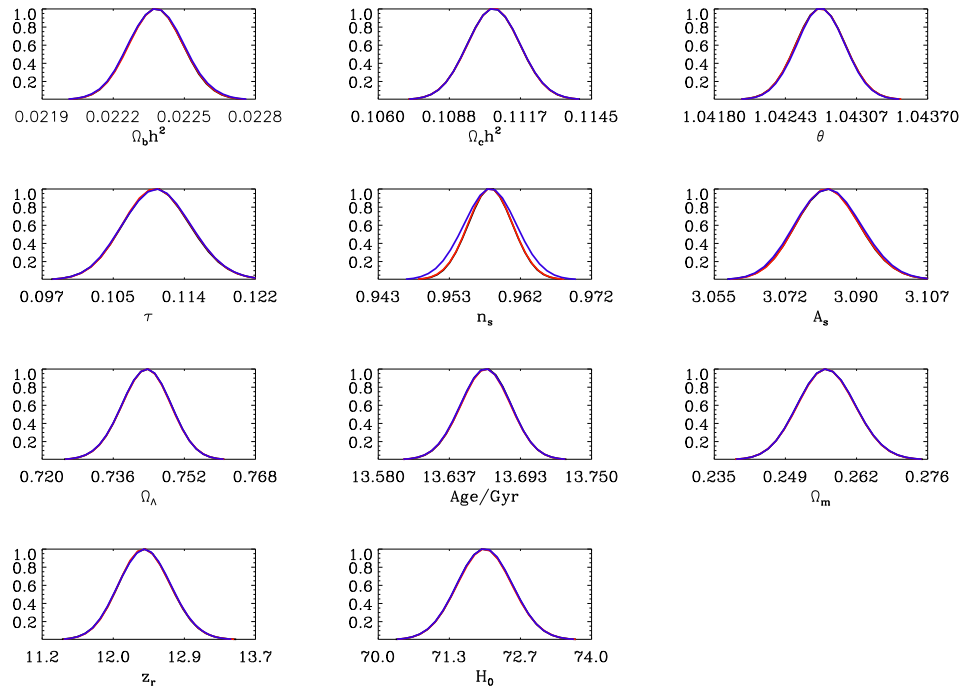


Figure 12. Marginalized parameter constraints for Planck 143 GHz without beam uncertainty (black), marginalized over the beam uncertainty MCBR considering the destriped data (red) and in the presence of white noise + $1/f$ noise (blue).

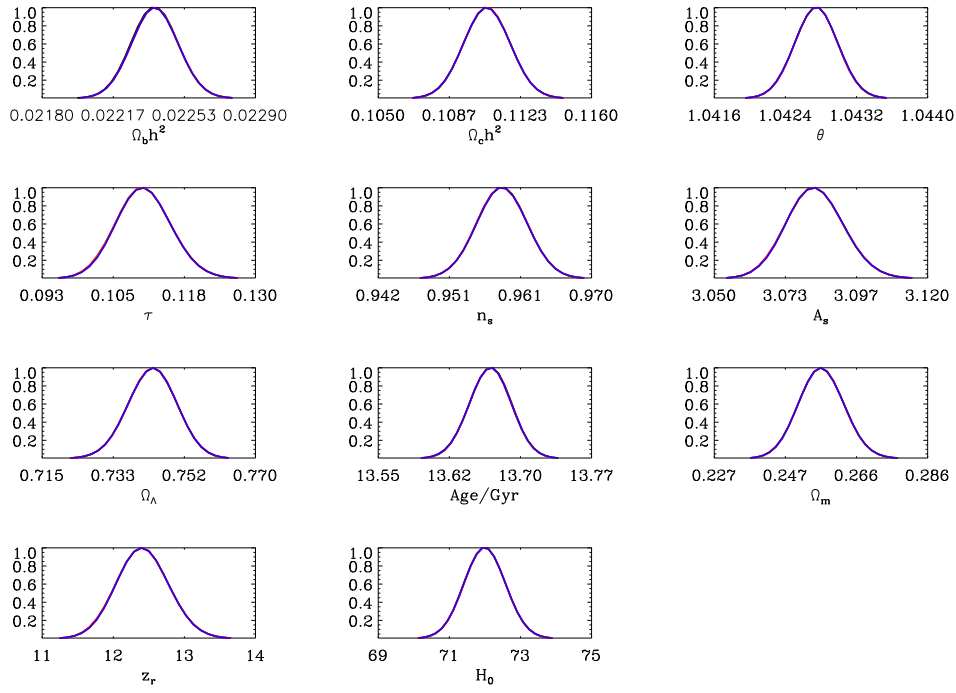


Figure 13. Marginalized parameter constraints for Planck 217 GHz without beam uncertainty (black), marginalized over the beam uncertainty MCBR considering the destriped data (red) and in the presence of white noise +1/f noise (blue).

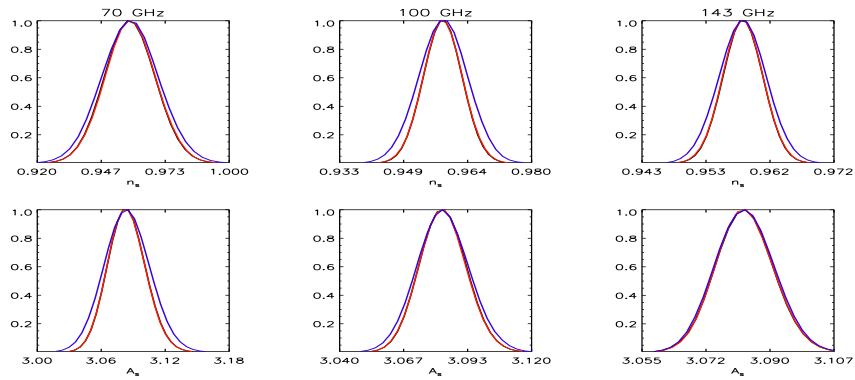


Figure 14. Marginalized constraints for the most impacted parameters, n_s and A_s , for Planck channels 70GHz, 100GHz and 143GHz, without beam uncertainty (black), marginalized over the beam uncertainty considering the destriped data (red) and in the presence of white noise +1/f noise (blue).

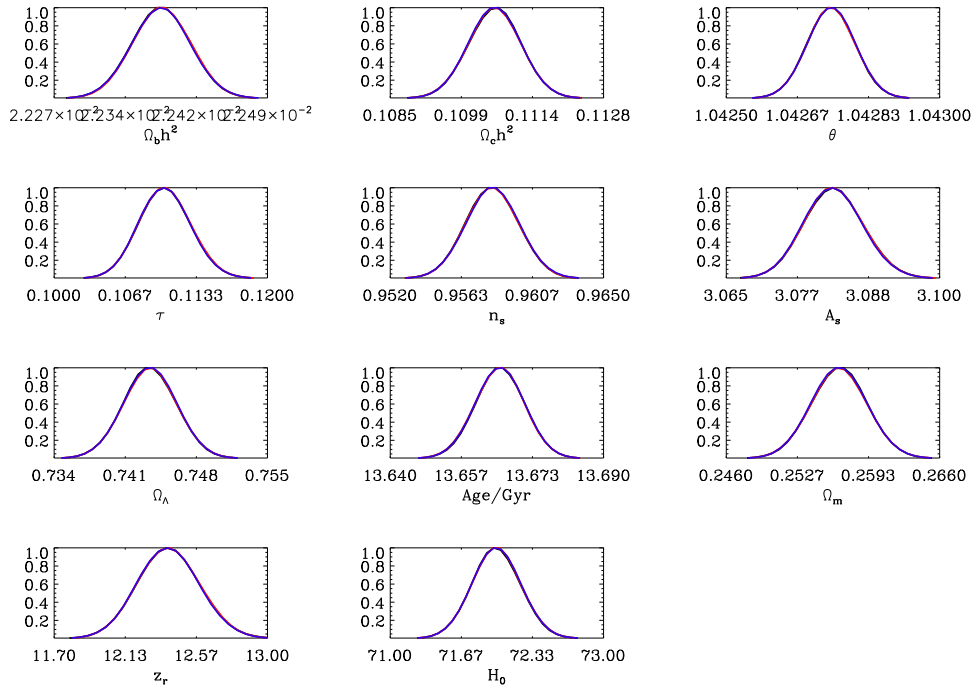


Figure 15. Marginalized parameter constraints for a future experiment with Epic 150 GHz specifications without beam uncertainty (black), marginalized over the beam uncertainty considering the desriped data (red) and in the presence of white noise + $1/f$ noise (blue).

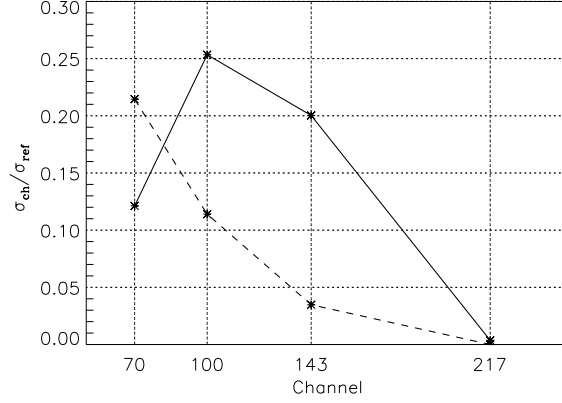


Figure 16. Enhancement factor, σ_{ch}/σ_{ref} for n_s (solid line) and A_s (dashed line), where σ_{ch} is the width of the distribution when beam errors are marginalized over by applying MCBR; σ_{ref} is the width of the distribution for the simulated data convolved with the fiducial beam (no beams errors included), for beams fitted on data with white and $1/f$ noise background.

parameters, particularly n_s . This is mostly due to incomplete marginalization, as we do not encompass an adequate distribution of deviations from the chosen fitted transfer function.

For comparison, Figures 21 and 22 show marginalized parameter constraints for the 100 GHz and 143 GHz channels, respectively, on data that have not been destriped.

Figure 23 shows the bias in n_s and A_s as a function of the extreme beams fitted on destriped data. We consider the error on B_ℓ given by $(r_\ell - 1)$ for $\ell = 1/\sigma$ representing the sigma of the beam. The corresponding values are given in Table 3. For example for 100 GHz an uncertainty of the extreme beam transfer function b_ℓ^2 for $\ell = 810$ of $\approx 0.1\%$ bias the likelihood by 0.3σ and 0.13σ for n_s and A_s respectively. A beam transfer function known up to 0.02% will bias n_s by 0.1σ . If we had not taken into account the beam uncertainties, then the same deviation in the transfer functions would have biased n_s by as much as 0.4σ , as can be inferred from Figure 16. The inadequacy of a likelihood that does not integrate the beam uncertainties is mentioned in (Huffenberger et al. 2009). There a simplified analysis of noisier data (only 1 horn) with all parameters except n_s fixed indicated that limiting the bias to 0.1σ would require knowledge of b_ℓ^2 to 0.04% where it has fallen to 1% of peak ($\ell \approx 1900$ for 100 GHz). In our analysis here we see that at $\ell \approx 1900$ an uncertainty of 0.5% for the extreme function would bias n_s by 0.3σ , while a mild deviation of the order 0.2% would produce a bias below 0.05σ (see Table 2). Hence a beam deviation five times that reported in (Huffenberger et al. 2009) would bias n_s by less than 0.1σ . This improvement is mostly due to properly marginalizing over the beam uncertainties via the MCBR method.

| ch | ℓ | r_ℓ^2 | $bias/\sigma (n_s)$ | $bias/\sigma (A_s)$ |
|-----|--------|------------|---------------------|---------------------|
| 70 | 579 | 1.00217 | 0.1890 | 0.2846 |
| 100 | 810 | 1.000928 | 0.3282 | 0.1240 |
| 143 | 1141 | 1.000982 | 0.3775 | 0.1055 |
| 217 | 1620 | 1.00043 | 0.0929 | 0.0188 |

Table 3. Bias on n_s and A_s in units of the error due to the deviation of the extreme function $(r_\ell^{ext})^2$ at $\ell = 1/\sigma$, after MCBR, fitted on destriped data. For each Planck channel.

6. Conclusions

We have developed a fast new method, MCBR, to propagate beam uncertainties to parameter estimation. The method properly accounts for the marginalised errors in the parameters. A desirable feature of the method is that it makes minimal assumptions on beam uncertainties. For example, it does not assume the data are normally distributed, and, unlike other approaches such as analytic marginalization, it does not require Gaussian priors on the specific systematic uncertainty. Furthermore it accounts accurately for the shape of the beam as it makes use of beam uncertainty templates for such beams, hence there is no need for simplified a priori assumptions on their shapes. Finally MCBR can be generalized and used to propagate other systematic uncertainties, as long as a set of templates of such systematics is provided.

From the study presented here on propagating the beam measurement errors to parameter estimation via the new MCBR method for Planck and for a future experiment, we conclude:

- Removal of $1/f$ noise residuals, by destriping or other techniques, is quite important.
- The main impact of beam uncertainties is to widen the marginal distributions of some parameters (most notably n_s).

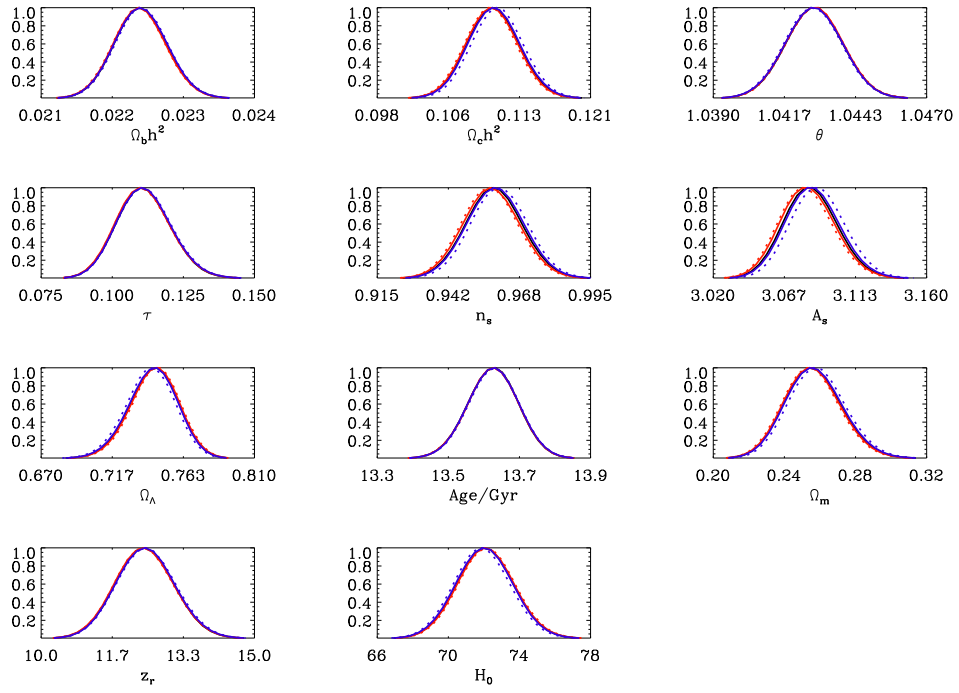


Figure 17. Marginalized parameter constraints for Planck 70 GHz with beam randomization MCBR: true beam (black), decreasing function for destriped data (red), increasing function for destriped data (blue), mild deviation (solid line) and extreme deviation from the true beam (dotted line)

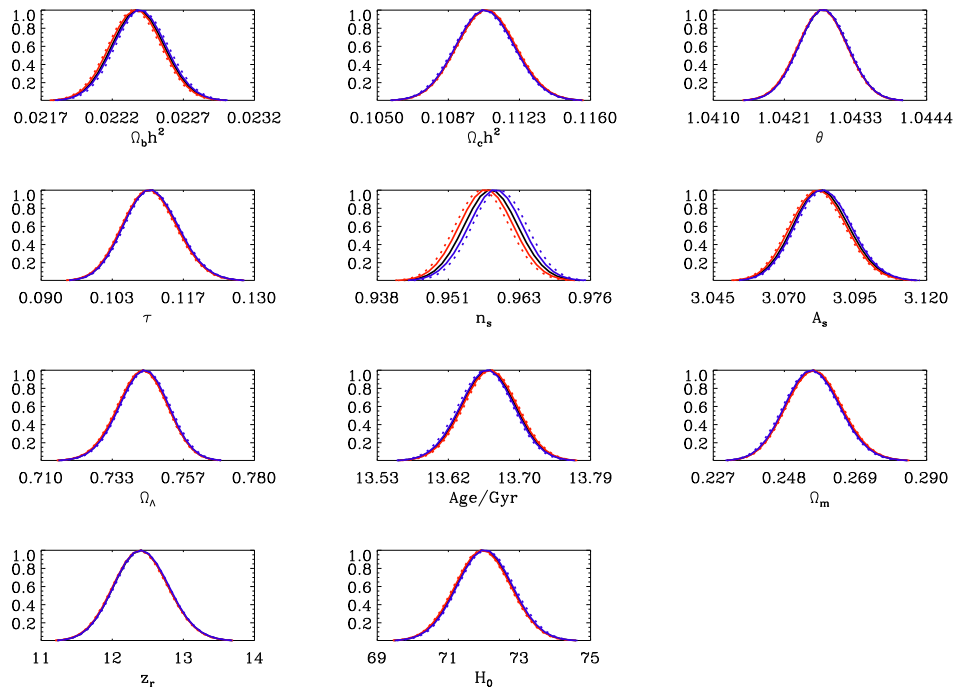


Figure 18. Marginalized parameter constraints for Planck 100 GHz with beam randomization MCBR: true beam (black), decreasing function for destriped data (red), increasing function for destriped data (blue), mild deviation (solid line) and extreme deviation from the true beam (dotted line)

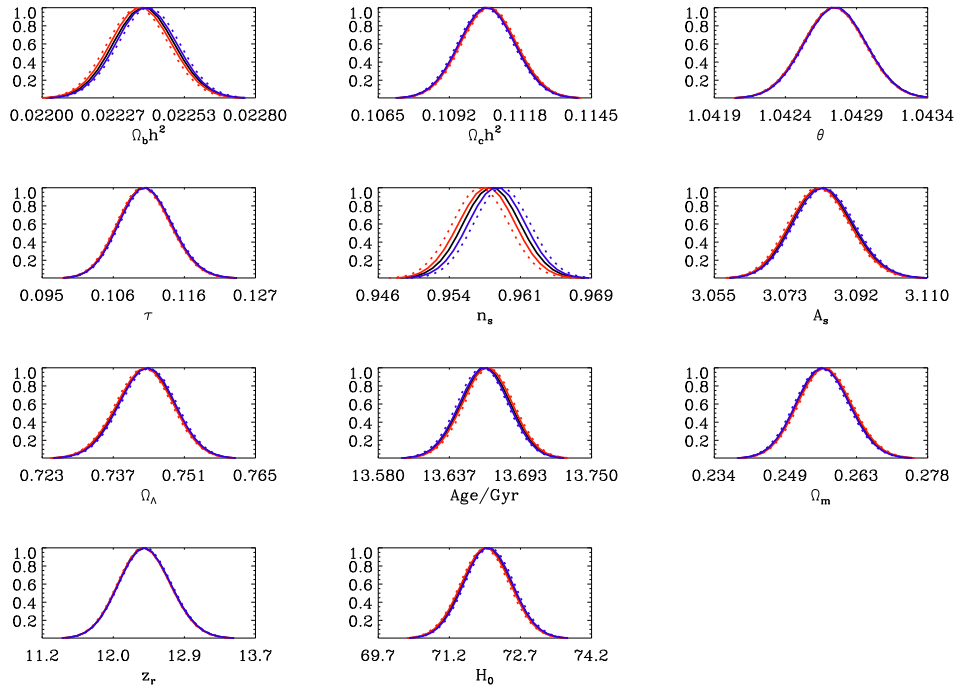


Figure 19. Marginalized parameter constraints for Planck 143 GHz with beam randomization MCBR : true beam (black), decreasing function for destriped data (red), increasing function for destriped data (blue), mild deviation (solid line) and extreme deviation from the true beam (dotted line)

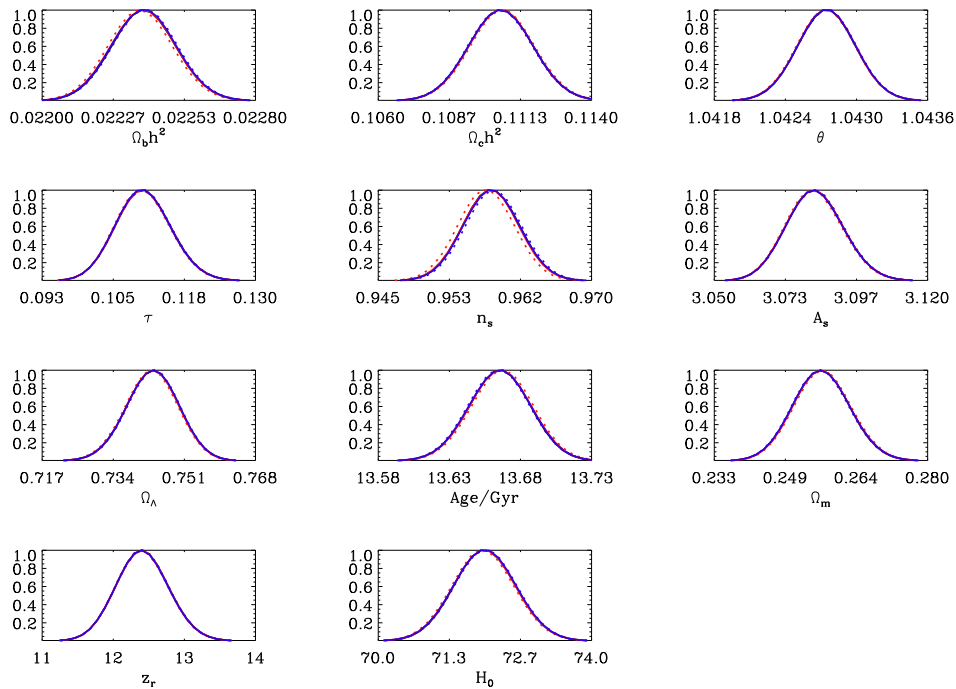


Figure 20. Marginalized parameter constraints for Planck 217 GHz with beam randomization MCBR: true beam (black), decreasing function for destriped data (red), increasing function for destriped data (blue), mild deviation (solid line) and extreme deviation from the true beam (dotted line)

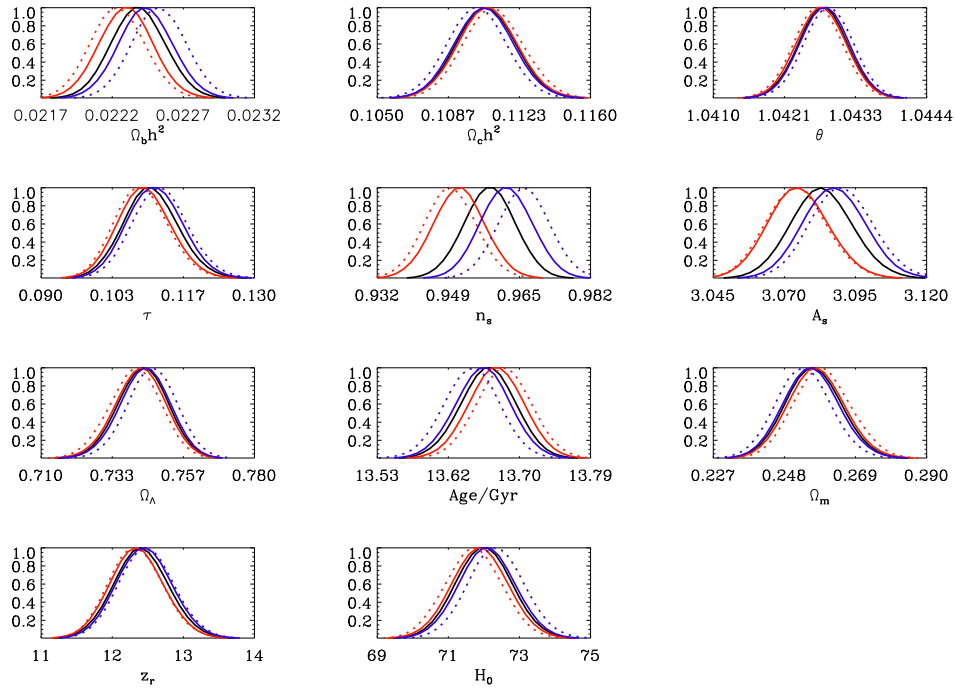


Figure 21. Marginalized parameter constraints for Planck 100 GHz with beam randomization MCBR: true beam (black), decreasing function for white +1/f noise (red), increasing function for white +1/f noise (blue), mild deviation (solid line) and extreme deviation from the true beam (dotted line)

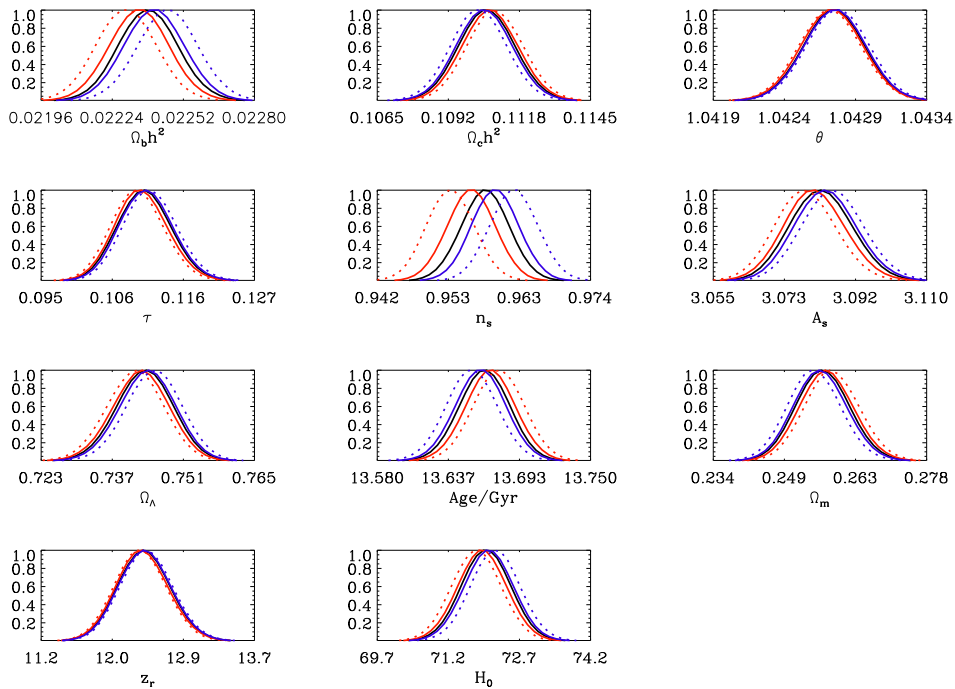


Figure 22. Marginalized parameter constraints for Planck 143 GHz with beam randomization MCBR: true beam (black), decreasing function for white +1/f noise (red), increasing function for white +1/f noise (blue), mild deviation (solid line) and extreme deviation from the true beam (dotted line)

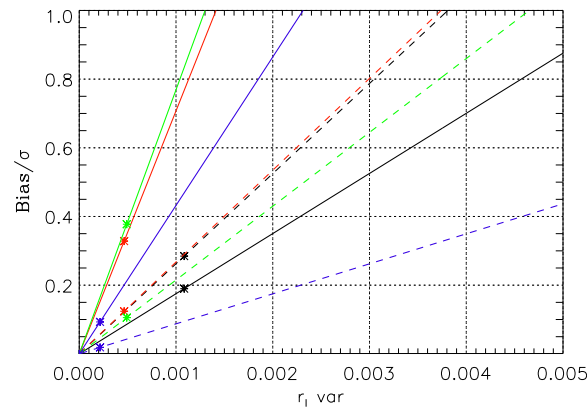


Figure 23. Bias on n_s (solid line) and A_s (dotted line) in units of the error for the extreme beam functions, r_ℓ^{ext} for $\ell = 1/\sigma_v$ after beam randomization MCBR, fitted on destriped data. For 70GHz (black), 100GHz (red), 143GHz (green) and 217GHz (blue).

- Assuming as extreme beam deviation in the simulated data results in a biased estimation of some parameters (mainly of n_s) due to incomplete marginalization.
- The parameters more noticeably impacted by beam uncertainties are: n_s , $\Omega_b h^2$ and A_s

These results demonstrate the relevance of applying destripping techniques on Planck data to remove $1/f$ noise.

When the beam fitting is performed in destriped data the uncertainties on the beams for say 100GHz are at most of the order of 0.5% for $\ell = 1500$ which translates into an increase of parameter uncertainties at most of the order of 0.1%. Instead the uncertainties on A_s at 70GHz and on n_s at 100GHz increases approximately by 20% and 26% respectively for beams fitted on white + $1/f$ noise data while it remains unaltered for white noise background alone.

The effect of wrong assumptions on beam parameters will bias the parameter constraints only for extreme deviations from the true beam and hence for quite atypical circumstances. Considering the analysis performed on destriped data, at 100 GHz an uncertainty of the extreme beam transfer function at $\ell = 810$ of $\approx 0.1\%$ will bias the likelihood by 0.3σ and 0.13σ for n_s and A_s , respectively. A beam transfer function known to 0.02% will bias n_s by 0.1σ . If we had not taken into account the beam uncertainties, then the same deviation in the transfer functions would have biased n_s by as much as 0.4σ . To limit the bias in n_s to less than 0.1σ will require a knowledge of a mild deviated beam b_l^2 to 0.2% where it has fallen to 1 percent. A mild deviated function gives rise to no observable bias (ie at most of the order 0.05σ).

Therefore we expect only a small impact of beam measurement errors on cosmological parameter estimation as long as the beam fitting is performed on destriped data.

Acknowledgements. GR is grateful to Jeffrey Jewell and Lloyd Knox for insightful discussions. LP acknowledges support by ASI contract I/016/07/0 "COFIS". KMH receives support from NASA via JPL subcontract 1363745. We gratefully acknowledge support by the NASA Science Mission Directorate via the US Planck Project. The research described in this paper was partially carried out at the Jet propulsion Laboratory, California Institute of Technology, under a contract with NASA. Copyright 2009. All rights reserved.

References

- Ashdown M. A. J., CTP *et al* *Astron. Astrophys.* **467** (2007a) 761 [arXiv:astro-ph/0606348].
 Ashdown M. A. J., CTP *et al* *Astron. Astrophys.* **471** (2007b) 361 [arXiv:astro-ph/0702483].
 Ashdown M. A. J., CTP *et al* *Astron. Astrophys.* **493** (2009) 753 [arXiv:astro-ph/08063167].
 Bock J. *et al.*, [arXiv:astro-ph/0805.4207].
 Bond J. R., Jaffe A. H., Knox L., 2000, *ApJ*, **533**, 19
 Bridle S. R.; Crittenden R.; Melchiorri A.; Hobson M. P.; Kneissl R.; Lasenby A. N., *MNRAS* **335** (2002)1193B
 Fendt W. A. and Wandelt B. D., *Astrophys. J.* **654** (2006) 2 [arXiv:astro-ph/0606709].
 Huffenberger K. M. *et al.*, *A&A* (2009) (submitted)
 Lewis A. and Bridle S., *Phys. Rev. D* **66** (2002) 103511 [arXiv:astro-ph/0205436].
 Lewis A., Challinor A. and Lasenby A., *Astrophys. J.* **538** (2000) 473 [arXiv:astro-ph/9911177].
 Lewis A., *Phys. Rev. D* **71** (2005) 083008 [arXiv:astro-ph/0502469].
 Maffei *et al* 2009, in prep.
 Planck Collaboration, Planck Blue Book, [arXiv:astro-ph/0604069].
 Poutanen T., CTP *et al* *Astron. Astrophys.* **449** (2006) 1311 [arXiv:astro-ph/0501504].
 Rocha G., Magueijo J., Hobson M., Lasenby A., *Phys. Rev. D* **64** (2001) 063512 [arXiv:astro-ph/0008070].
 Sandri M., Bersanelli M., Burigana C. *et al.* 2002, in American Institute of Physics Conference Series, Vol. 616, Experimental Cosmology at Millimetre Wavelengths, ed. M. de Petris & M. Gervasi, 242-244
 Sandri M. *et al* 2009, in prep.
 Spergel D. N. *et al.* [WMAP Collaboration], *Astrophys. J. Suppl.* **148** (2003) 175 [arXiv:astro-ph/0302209].
 Yurchenko V. B., Murphy J. A., & Lamarre J.-M. 2004, Proceedings of the SPIE, Volume 5487, pp. 542-549 (2004), ed. J. C. Mather, 542-549